Evidence of conformational landscape alteration and macromolecular complex formation in the early stages of in vitro human prion protein oxidation

Frédéric Halgand, Jan Bohl, Cécile Sicard, Human Rezaei, Guillaume van Der Rest

Evidence of conformational landscape alteration and macromolecular complex formation in the early stages of in vitro human prion protein oxidation.

Jan Bohl [a], Cécile Sicard [a], Human Rezaei [b], Guillaume Van der Rest [a], Frédéric Halgand [a]*

[a] Université Paris-Saclay, CNRS, Institut de Chimie Physique UMR 8000, 91405 Orsay, France.
[b] Institut National de la Recherche Agronomique, UR892, Virologie Immunologie Moléculaires, Domaine de Vilvert, 78350 Jouy-en-Josas, France.

Abstract: 260 words
Oxidative stress is proposed to be one of the major causes of neurodegenerative diseases. Cellular prion protein (PrP) oxidation has been widely studied using chemical reagents such as hydrogen peroxide. However, the experimental conditions used do not faithfully reflect the physiological environment of the cell. With the goal to explore the conformational landscape of PrP under oxidative stress, we conducted a set of experiments combining the careful control of the nature and the amount of ROS produced by a ^{60}Co γ-irradiation source. Characterization of the resulting protein species was achieved using a set of analytical techniques. Under our experimental condition hydroxyl radical are the main reactive species produced. The most important findings are i) the formation of molecular assemblies under oxidative stress, ii) the detection of a majority of unmodified monomer mixed with oxidized monomers in these molecular assemblies at low hydroxyl radical concentration, iii) the absence of significant oxidation on the monomer fraction after irradiation. Molecular assemblies are produced in small amounts and were shown to be an octamer. These results suggest either i) an active recruitment of intact monomers by molecular assembliesô oxidized monomers then inducing a structural change of their intact counterparts or ii) an intrinsic capability of intact monomer conformers to spontaneously associate to form stable molecular assemblies when oxidized monomers are present. Finally, abundances of the intact monomer conformers after irradiation were modified. This suggests that monomers of the molecular assemblies exchange structural information with intact irradiated monomer. All these results shed a new light on structural exchange information between PrP monomers under oxidative stress.

Keywords: oxidative stress, gamma irradiation, prion protein, ion mobility, mass spectrometry.

1. Introduction:

Increased damages caused by free radicals are found in prion-infected brain tissues, thus suggesting that oxidative stress has a pivotal role in prion pathologies [1, 2]. Oxidative stress which is known to increase with age, was also found to be related to sporadic forms of prion diseases [3] as well as the occurrence of other amyloidogenic diseases such as Alzheimer's [4, 5] or Parkinson's diseases [6]. Among the molecular species responsible for *in vivo* oxidation, the hydroxyl radical ($OH^{\dot{A}}$) has the highest oxidation potential and is prone to oxidize cellular components. A source for hydroxyl radical production *in vivo* is the metal-catalyzed oxidation (MCO) induced by copper and iron ions in the presence of H_2O_2. Copper-catalyzed oxidation on human prion protein (PrPhu = PrP^C) bound with copper ions can be summarized as leading to dimerization and fragmentation of the protein [7]. A number of studies have focused on *in vitro* oxidation of PrP^C (see Table 1) as it is an excellent target for oxidation due to the presence of several amino-acid residues particularly susceptible to oxidation such as methionine. Indeed, oxidation of methionine residue 205 in PrP^C was shown to lead to a drastic change in the secondary to tertiary structures of PrP^C [8, 9]. Oxidized PrP^C is typically richer in β-sheets than non-oxidized PrP^C [8-13]. Rich β-sheets monomers were also correlated to aggregation, neurotoxicity enhancement [8, 9, 12], and to β-cleavages [1, 14]. In these studies, as for other protein systems, the most common reagent used to probe oxidative stress is H_2O_2. To achieve enough oxidation, H_2O_2 is introduced in large excess compared to the protein concentration, and reaction is often performed at the physiologically relevant temperature of 37°C either with or without metals to promote MCO [8, 9, 11, 12]. The nature of the oxidation products is usually documented using biochemical methods coupled with mass spectrometry [11, 13]. Since oxidation by H_2O_2 is challenging to control and considering that the addition of reagents could change the protein medium, ionizing radiations can be used to generate selected reactive oxygen species (ROS) in controlled concentrations [15-17]. In this kind

---

Abbreviations: PrPhu and PrPC: Full length human prion protein ; IM: Ion mobility; CCS: Collision cross section; ROS: Reactive oxygen species.

This work was supported with the funding by the Ile-de-France DIM Analytics program for the MOBICS project.

* Corresponding author: Dr F. Halgand, Université Paris-Saclay - CNRS, UMR 8000, Rue Ampère, Bâtiment 201P2, 91405 Orsay, France. Phone: +33 1 69 15 82 51.
Email address :frederic.halgand@universite-paris-saclay.fr

of radiation, radicals are furthermore produced and spread out homogenously in the solution.

With these previous results in mind, it was of interest to apply the methodology that we recently described to probe the effect of protein concentration changes on the conformational landscape of the prion protein [18] in order to investigate the early stages of oxidation of the human prion protein, which might also affect intermediate oligomeric species. This methodology is based on the use of native electrospray ionization mass spectrometry (ESI-MS) which has become a valuable tool for the study of protein associations [19, 20]. Native ESI-MS makes it possible to generate important pieces of information about protein complexes such as their stoichiometry or the assembly mechanism [21-23] by rigorously controlling experimental parameters to preserve native structures in the gas phase [24, 25]. More recently, the coupling of ion mobility devices to commercial mass spectrometers added another analytical dimension to MS, then opening new possibilities for MS in the field of structural biology [26, 27]. Briefly, ion mobility spectrometry (IMS) differentiates molecules according to their collision cross section (CCS), charge (z) and shape and makes it possible to separate isobaric protein or peptide ions [28-32]. IMS-MS has been successfully applied to examine protein-ligand [33] and protein-protein [34, 35] interactions as well as intrinsically disordered protein characteristics [27, 36-39].

Thus, with the aim at exploring tertiary and quaternary properties of PrP under oxidative stress and the degree of conformational changes under oxidative stress conditions, we conducted a set of experiments using controlled doses of γ-irradiation, producing sub-stoichiometric amount of $OH^{\check{o}}$ in the absence of O_2. The characterization of the resulting oxidized prion species was achieved using various physico-chemical methods including size exclusion chromatography coupled to ion mobility and mass spectrometry (SEC-IMS-MS), sodium dodecyl sulfate polyacrylamide gel electrophoresis (SDS-PAGE), atomic force microscopy (AFM), and circular dichroism (CD). The most important finding relies to the detection of molecular assemblies (octamer) containing a majority of non-modified monomer mixed with oxidized monomers under sub-stoichiometric amounts of $OH^{\check{o}}$. This result indicates either an active recruitment of intact monomers (unmodified, not oxidized) by molecular assembliesô oxidized monomers or an intrinsic capability of intact monomer conformers to spontaneously associate to their oxidized counterparts. Finally, abundances of the intact monomer conformers were modified under oxidative stress. This suggests that monomers of the molecular assemblies exchange structural information with intact monomer.

2. Material and methods:

2.1. Material

2.1.1. Production of PrP proteins

Full length PrP or ARQ was expressed in *E. coli* and purified as described previously [40]. Briefly, the gene encoding full-length PrP was cloned in a pET 22b+ vector and expressed in a BL21 DE3 *E. coli* strain after isopropyl ɓ-D-1-thiogalactopyranoside (IPTG) induction. After lysis, sonication and solubilization of the formed inclusion bodies by guadinium chloride, purification of the prion protein was performed on a Ni Sepharose column.

Refolding of the protein was achieved on an affinity column (Amersham Biosciences sephadexTM G25, Volume 400 mL, ÄKTA Purifier, conductometer and UV cell at 220 nm and 280 nm, GE Superloop 250 mL) by heterogeneous phase renaturation simultaneously with purification on Sepharose beads loaded with Ni^{2+}. The protein was eluted with ammonium acetate buffer (CH_3COO^- NH_4^+) = 0.5g/L, pH: 4.5-5, 3ml/min). The proteins were lyophilized for long term storage (Thermo Savant, RUA FROID BIO Micro Modulyo YO-230ò).

2.2. Methods

2.2.1. Protein irradiation

Irradiations were performed using a ^{60}Co γ–source. Reactive species are obtained by radiolysis of the dedicated solution, where the buffer composition, the pH and the irradiation dose were adjusted to control the nature and the production rate of the ROS. Irradiated PrP was diluted from a concentrated stock solution to a final concentration of 100 µM in 5 mM Phosphate solution at pH 3.9 (N_2O saturated). Under our experimental conditions, hydroxyl radicals are the main ROS produced in an anaerobic environment, as air is replaced by N_2O to scavenge and transform solvated electrons into $OH^{Å}$. Samples were irradiated with doses from 15 to 100 Gy. Under our conditions an irradiation dose of 100 Gy generates a cumulative hydroxyl radical ($OH^{\check{o}}$) concentration of 55 µM as electrons are scavenged by N_2O to generate $OH^{\check{o}}$. Control samples were identically prepared but not subjected to irradiation [16, 17]. Since its reaction rate is extremely fast $OH^{\check{o}}$ will only react with proteins in its surrounding as well as with accessible residues inside proteins. In our conditions, the radiation doses are not saturating. Radiation induces the formation of oxidized products that are formed linearly with the dose. But when these species concentration is high enough, they get oxidized a second time. Then, the production of the species bearing a single oxidation in not proportional to the dose anymore.

2.2.2.Size exclusion chromatography

To separate the protein samples prior to MS analysis a SEC column was coupled to the MS (TSK 2000 SW gel filtration column (Interchim), 4.6 x 300 mm). 10 µl of the irradiated samples were injected on the column and eluted with Triethylammonium Acetate (TEAA, 20 mM, pH 3.3) at a flow rate of 500 µl/min, with concomitant UV detection while $1/10^{th}$ of the flow was diverted to the mass spectrometer to record IMS-MS data. For denaturing condition analysis SEC was used to separate all species and protein denaturation was obtained using a 1/1 mixing solution of acetonitrile, water and formic acid (90/10/0.1 %, v/v) with SEC buffer prior to injection in the ESI source of the mass spectrometer.

2.2.3.Mass spectrometry analysis

Mass spectrometry experiments were performed on a QToF instrument (Synapt G2-Si HDMS, Waters Company, Manchester, UK). Acquisition of mass spectra were carried out over the *m/z* 500 to 5,000 mass range and analyzed in positive ion mode under ñnativeò and denaturing conditions. For ñnativeò experiments, instrumental and hardware parameters were optimized to reach the best average signal to noise ratio while preserving intact quaternary and tertiary structures. Ion mobility data were recorded in parallel. For analysis in native conditions the following instrumental parameters were used: capillary voltage = 4.5 kV, sampling cone = 150 V, source offset, 150 V, nebulization gas pressure = 5 bar, source temperature, 40 °C, desolvation temperature, 75 °C. For ion mobility experiments in nitrogen as drift gas, the following instrumental parameters were used: Trap gas flow = 7 ml/min; He gas flow = 120 ml/min, IMS gas flow = 45 ml/min, Trap wave velocity = 300 m/s, Trap wave height = 4 V, IMS wave velocity = 800 m/s, IMS wave height = 40 V, Transfer wave velocity = 110 m/s and Transfer wave height = 4 V. For denaturing conditions, ion mobility data were not recorded, and instrumental parameters were the following: capillary voltage = 1.5 kV, sampling cone = 50 V, source offset, 30 V, nebulization gas pressure = 6.5 bar, source temperature, 110 °C, desolvation temperature, 600 °C. Calibration was performed using sodium trifluoroacetate clusters. Averaged RMS deviation was around 0.5 to 10 ppm for ñnativeò full length PrP.

2.2.4.Data analyses, processing and interpretation of ion mobility experiments

After recording ion mobility data, we extracted mass to charge ratios (*m/z*), drift times (t_d) and intensities, using the peak detection procedure of Driftscope™ software. All the data were gathered in a raw data file (.csv). Then our home-made script [27] allowed extracting information only related to the protein of interest by entering its average molecular mass, the *m/z* accuracy, the limits of the charge states distribution as well as collisional cross section (Ω = CCS = collisional cross sections) calibration parameters. This allowed us to rapidly process the data and plot Ω = f (z) (Ω = CCS = collisional cross sections; *z* = charge state) graphs to reveal the conformational landscape of PrP. Calibration of TWIM based systems to provide absolute collision cross section for proteins is still an issue [41, 42] and this article does not aim to resolve it. Since no external data is available that would require absolute collisional cross section determination, this article is focused on qualitative and quantitative changes observed for conformer families. Therefore, calibration was done using data for myoglobin, following the protocol described by Ruotolo *et al.* [43] and the recommendation of Shvartsburg & Smith [44] to choose multiply charged proteins covering the expected mass range and cross-section ranges. To verify the reproducibility of our results the calibration of myoglobin was conducted based on three independent datasets. From the average q (z) values calculated for each mobility peak of each charge state a standard deviation (σ) of +/- 11.31 $Å^2$ was observed. In Figure S1, one can clearly observe that some charge states seem to be related to other neighboring charge states forming series of points that we will denote as conformer families (CF). In this denomination, we intend to convey that a single solution-phase conformation is expected to lead to a gas phase charge state distribution with CCS that should be closely related, and with a progression in CCS related to an increase in volume due to increased coulombic repulsion as charge states increase (see for instance Beveridge *et al.*[45]). This term is not totally accurate as one could expect that several conformations might be present in a single conformer family. In a quantitative point of view, for each charge state and each protein concentration of each ovine PrP, intensities at the peak apex of the arrival time distribution were automatically extracted. Summation of maximum ion mobility peak intensities for the specific drift time and charge state of each conformer family, allowed calculating the relative intensities (abundances) of each conformer family for each protein concentration. Extended information on this procedure is given in the Supporting Information section. Calculated standard deviations for the molecular assembly and monomer ratios intensities were 1.9% and 2.7%.

2.2.5.Circular dichroism

CD spectra were acquired on a spectropolarimeter (Jasco J710, JASCO, GER) using a quartz cuvette (Hellma, GER) with a path length of 0.5 mm. Irradiated PrP samples and a non-irradiated control were diluted to 30 µM in potassium phosphate buffer (20 mM, pH 3.9). The measurements were performed at a temperature of 25 °C. CD spectra were constructed based on eight consecutive scans.

2.2.6.SDS-PAGE

SDS-PAGE was conducted on Criterion TGX gels of 4 to 15% acrylamide gels (Bio-Rad, USA), which were loaded with 10 µl of 30 µM PrP in potassium phosphate buffer (20 mM, pH 3.9) mixed with to 10 times Laemmli buffer in volume with and without DTT. The gels were revealed with Coomassie staining.

2.2.7.Atomic Force Microscopy images

Irradiated prion samples were diluted to 200 nM in potassium phosphate buffer (20 mM, pH 3.9 or 7.0). Next, 40 µl of the diluted sample were deposited on a mica surface (MICA V-1 Grade, 9.5mm x 0.15 mm, Structure Probe INC., West Chester, PA, USA) glued to a microscope slide. After 5 minutes the surface was washed and immersed in water for analysis. Force images were acquired on a NanoWizard IV AFM (JPK Instruments AG, GER) in standard QI-mode using a BioLever mini cantilever (BL-AC40TS-C2, spring constant: 0.09 N/m, Resonance frequency: 110 kHz, Olympus, JP). Images were treated by one polynomial line fit and a histogram line fit using the data processing software of the AFM (JPK data processing, Version spm-6.1.59, JPK Instruments AG, GER).

3. Results

This study emerged in part from the fact that prior articles of reference reporting the study of oxidative stress on prion protein used large amounts of reagents such as hydrogen peroxide (See table 1). With the view to better mimic *in vivo* oxidative stress conditions, we chose to study the effect of hydroxyl radicals, produced by a gamma irradiation source in anaerobic conditions, which is rarely the case for *in vivo* studies but closer to oxygen concentrations in the cell, and for irradiation doses leading to a total cumulated concentration of hydroxyl radicals below or equivalent to the protein concentration (< 100 µM). Hydroxyl radical reacts on biological compounds with reaction rates of 10^{10} to 10^{8} $M^{-1}.s^{-1}$ [15, 46-48], thus the instantaneous concentration remains very low but higher reaction yields can be controlled by the cumulative radiation dose received by the sample. With the ^{60}Co γ-irradiation source used in this work for $HO^{\bullet}$ production in the absence of O_2 and in the presence of N_2O, 1 Gy (1 $J.kg^{-1}$) of radiation leads to the formation of 0.55 µM of $HO^{\bullet}$. Thus, the maximal dose of 100 Gy used for this work amount to a maximum cumulative concentration of 55 µM.

In initial experiments irradiations were conducted both at neutral and acidic pH. At pH 7, major precipitation of the sample was observed even for the lowest irradiation doses. Under these conditions we were not able to detect any prion monomer. In order to look for remaining soluble forms the solution was spun (12000 g, 30 min) and the supernatant analyzed. No prion protein was observed in the supernatant in these conditions. No tendency to precipitate at pH 3.9 was observed after irradiation, and we never observed any precipitate in vials and detection by mass spectrometry was always good. Attempts were also done to reduce the protein concentration in order to slow the precipitation process. Down to 20 µM, the minimum for which all experiments could be conducted, and following the same protocol as for the original experiments, precipitation was still observed upon irradiation at pH 7. Consequently, since no precipitation was observed at pH 3.9, this condition was chosen for all further experiments.

After γ-irradiation of PrP^{C}, the protein samples were separated by SEC, with a UV detection at 280 nm and ionized in the ESI source of the IM-MS instrument. Both UV, IMS and MS data were recorded. Size exclusion chromatography revealed that irradiation induced the formation of larger size molecular assemblies (MA) of PrP^{C} having an elution time of 29.3 minutes faster than dimers (37.0 minutes) and monomeric PrP (Mirr, 41.1 minutes) (see Figure 1 A). The relative monomer ratios detected during SEC declined slightly by approximately 15 % with increasing irradiation doses and stabilized for 50 Gy and higher irradiation doses (see Figure 1 B and Figure S2). Dimers were observed for the control sample in SEC-MS chromatograms as well as in the irradiated samples. SDS-PAGE gels conducted with and without DTT (Figure 2A) show that for the control sample, nearly no dimer band is observed in the presence of DTT whereas a strong dimer band is observed in the absence of DTT. This points towards artefactual formation of dimers by cysteine bridge cross-protein swapping occurring through the expression and purification processes[49]. The dimer intensity increased by approximately 7.5% with increasing irradiation doses. Part of this dimer therefore seems to be formed during irradiation. Higher molecular weight species, MA, were observed even for low irradiation doses (7 Gy = cumulative concentration of 3.85 µM $OH^{\bullet}$ compared to 100 µM protein concentration) but in very weak amount that only allowed to distinguish some peaks of the MA but do not permit its conformational analysis. For irradiation doses up to 50 Gy (50 Gy = cumulative concentration of 27.5 µM $OH^{\bullet}$ compared to 100 µM protein concentration), the relative intensity of MA increased to reach approximately 7.5% and slightly decreased for higher doses (Figure 1 B & C). This decrease could be caused by some precipitation. Samples treated with 0, 7, 25, and 100 Gy irradiation doses were loaded on SDS-PAGE gel under denaturing conditions (Figure 2 A). Most of the protein was detected as monomers and dimers increasing with the dose. Since the whole denatured sample was loaded without separation on the gel, the dimers could originate from both the molecular assemblies and the dimers separated in SEC. This indicates that the

MA are non-covalent complexes composed of either monomers or dimers, and not of higher order covalent assemblies. However, ratios amount of the different species (M and MA) for each irradiation dose were estimated based on UV absorbances. Under these conditions, molecular assemblies represent approximately ~ 5% of the total signal intensity (Total Ion Chromatogram = TIC). This roughly correlates with the expected amount of theoretically observable oxidized PrP at 7 Gy, which lies around 3.85% of the total protein present and taking into account hydroxyl radical reactivity with the consumption of two hydroxyl radicals per oxidation [15], as well as the occurrence of other oxidation products thus lowering intensity signal. In addition, the limited increase of abundance species at higher irradiation doses might be due to precipitation which also applies to the molecular assemblies.

When specifically analyzing MS spectra under the chromatographic peaks (SEC) of MA and Mirr, we observed that the signal obtained from the chromatographic monomer fraction showed one charge state distribution ranging from CS +5 to +7 (Figure 2B and 2C), while, for molecular assemblies only peaks from monomer with a larger charge state distribution (CS +6 and +18) are observed (Figure 2B and 2D). Note that dimer did no display any change after irradiation (Figure S3). It is known that precipitates that dissociate in the ESI process or in the gas phase generally undergo an asymmetric fragmentation where one monomer unfolds and picks up most of the charges, leaving a multimer with a low charge and thus high *m/z* that is probably not visible in our instrument [50]. Thus, in this initial SEC-MS experiments, only multimer dissociation was observed. Native MS led to observe the monomer of the molecular assemblies (MAm) with a mass of 22 874 Da, an increase of 42 Da compared to the theoretical mass. This could have been an indication for the presence of modified species, but comparison of the monomer +6 CS peak in the control monomer (Mctrl) and intact irradiated monomer (Mirr) spectra also displayed the presence of numerous adducts in all native MS spectra (Data not shown). A solution to allow direct comparison of the MS spectra, with similar charge states and adduct formation for all the species present at various elution times and at various multimeric states is to proceed by on-line denaturation. Thus, our experimental setup was modified (Figure 2D) to include a mixing of the flow from the column with an equivalent flow of ACN:H_2O:formic acid (90:10:0.1; V/V). In these denaturing conditions, the major peak in the charge state distribution (CSD) is the +14 CS. This peak appears to contain three components for all conditions: the unmodified monomeric peak and increases of +16 Da and +37 Da relative to the unmodified peak. The first mass increment could indicate the presence of the addition of an oxygen atom (Figure 2C & 2D). Overlaying of the traces shows that both of the peak profiles between the irradiated monomer peak and the control monomeric peak do not show major differences in native conditions (Figure 2C insert). On the other hand, in denaturing conditions, the +14 CS peak shows an increase in abundance of the +16 Da and +37 Da adducts for MAm compared to the monomers (control or irradiated), in Figure 2D and insert. This result was reproducible for the different doses, with only little variation in the oxidization content with the dose. The observation that modified and non-modified monomers are detected in the MA corroborates the observation on the UV-DAD measurement where the higher signal intensity of MA at 7 Gy would require the inclusion of both oxidized and non-oxidized monomers in the MA. Such a heterogeneous formation of MA was unexpected and is reported here for the first time in the literature. Since size exclusion chromatography fractionation was run on a column calibrated in the range of 1 MDa to 20 KDa, thus allowing the estimation of the molecular weight of the molecular assembly to a value ranging from 110 to 150 kDa with an estimated averaged molecular weight of 137 ± 20 kDa. First using our initial ñnativeò conditions we were not able to detect the intact molecular assemblies. Under these experimental conditionsô oligomers dissociated in the gas phase to give rise to monomers. However, after careful tuning of the mass spectrometer, a CSD with an (CS +48 at *m/z* 3,806.4) average molecular weight of 182 kDa (see Figure 3) was observed, which corresponds to the mass of eight monomers. This species could quite well correspond the SEC data, and we therefore surmise that the molecular assembly detected in SEC is most likely an octamer. Note that part of this last also undergoes some gas phase dissociation with the presence of monomers having a CSD ranging from +9 to +22 CS.

The logical next stage was to attempt localization of the oxidation within the proteins included in this MA. The overall very low abundance of the MA (less than 2% of TIC intensity), the trend to precipitation for higher doses and presumably the diversity of chemical modifications induced by oxidation has led to the fact, that, despite our efforts carried out into this direction, we did not succeed in the identification of specific oxidation pattern within the MAôs, after collecting and concentrating several MA fractions.

Simultaneous recording of ion mobility and mass spectrometry data allowed a qualitative description of the conformational profile (Figure 4) of the monomers of the monomeric and molecular assembly fractions. To this goal drift times of the respective charge states and species (monomer from molecular assemblies = MAm and monomer from monomer fraction = Mirr) were converted in collisional cross section following a procedure described in the Material and Methods section and detailed in supporting information [27]. Ion mobility data can be

interpreted both in terms of qualitative and quantitative ways. Qualitatively and quantitively, it is impossible to compare the ion mobility patterns between M and MA since MA monomers come from a gas phase dissociation thus impairing the ion mobility profile of these last. Therefore, qualitatively, whatever the irradiation doses were, PrP conformational profiles were the same irrespective of the oxidation products (Figure 4A). Therefore, IMS data revealed that independently from the nature of the chemical modifications due to irradiation, no difference in the CCS was observed (see Figure 4) for a dedicated irradiation dose. The monomers of the molecular assemblies (MAm) present in each irradiated sample share therefore similar structures. This is exemplified with irradiation dose of 7 Gy. For higher irradiation doses of 25 and 100 Gy the CCS of the monomers embedded in the molecular assemblies were shown to structurally collapse (smaller CCS). This is in contrast with CCS observed for an irradiation dose of 7 Gy, that display higher CCS after irradiation in agreement with a more extended structure. It is also noticeable that monomer not embedded in molecular assemblies (intact monomer = Mirr = unoxidized monomer) after irradiation have similar CCSs compared to non-irradiated monomer (control = MCtrl). This result demonstrates that whatever the irradiation dose was, monomers (Mirr) representing the main species were qualitatively not affected (Figure 4A).

In contrast, comparison of mobility data between M and Mirr is possible since both monomers were analyzed under identical conditions and were submitted to the same experimental process, as demonstrated by the change in CF ratio intensities between these two species. Finally, for the dimer, since this last wasnôt modified under gamma irradiation (See Figure S3) its conformational properties were not investigated. Consequently, quantitatively the relative abundances of Mirr irradiated conformers compared to MCtrl, were shown to evolve with increasing irradiation doses: When the irradiation dose increased CF3 conformer abundance decreased while CF2 and CF1 conformersô abundances increased. This means that with increasing irradiation doses, CF3 conformer is consumed to the profit of CF2 and CF1 conformers. Finally, at the highest irradiation dose CF3 became the major conformer, a result that could be explain by precipitation / precipitation that led to new conformer abundances ratios (Figure 4B).

Circular dichroism was used to probe the nature and content in secondary structures in all species. First, CD was performed on the raw sample containing all species (see Figure S4). Results showed that no significant change in CD spectra occurred, indicating that PrP monomers embedded in molecular assemblies do not show a detectable modification in their secondary structure. The isolated samples (MA and Mirr) collected after SEC were too low in intensity to be analyzed with CD. To structurally characterize the generated PrP species, AFM images were recorded (see Figure 5). The difference between the images is represented by an increasing number of taller objects as exemplified with the image recorded at 25 and 100 Gy that displays the presence of objects having a height up to 10 nm (red color). This is also supported by evolution of the size of the species as illustrated with the bar graphs depicting the number of objects with respect to their height. Thus, it clearly appears that under irradiation at pH 3.9 a general trend with the emergence higher objects is observe. Note that at 200 Gy irradiation height profile of the entities is modified, a result assigned to precipitation of the largest objects. Consequently, the tendency is then that after oxidation, objects move towards taller objects. See Figure 5.

4. Discussion

More and more data support a causal link between oxidative stress and prion diseases. Indeed, PrP can be considered as an antioxidant protecting the cell against Reactive Oxygen Species (ROS) activity [51]. In healthy conditions, methionine sulfoxide reductase reverses the ROS oxidation of PrP [10]. However, in the case of a defect of this equilibrium, ROS were shown to promote neurotoxicity in neuronal cells, which is a hallmark of prion diseases [10]. In literature, oxidation of PrP has thought to mainly occur on methionine at residues 213, 205, and 206. Here, residue 206 has a key function since its oxidation promotes the exposition of the inner hydrophobic core leading to a general disruption of the protein structure [8, 12]. In these circumstances the oxidation process of PrP could be related to a loss of oxidative defense *in vivo* [51]. One should nevertheless keep in mind that, compared to previous work, the generation of ROS by γ-irradiation in the absence of oxygen strongly differs from metal catalyzed oxidation (MCO) mainly involving copper and iron and that the amounts of hydrogen peroxide produced under irradiation is negligible compared to those used for MCO.

Before discussing our results, we must review the relevance of working on a recombinant protein in terms of structure but also in relationship with the prion pathologies. The differences in the fold of recPrP and extractive PrP^C has been well investigated in the past through different biochemical techniques comprising NMR approaches. Precisely, this last technic used by Wuthrichôs group well demonstrated that the full-length extractive PrP^C and recPrP share the same α-fold [52]. This group also investigated the thermal unfolding of extractive PrP^C versus recPrP and showed similar thermal unfolding behavior even if they did not demonstrate its reversibility. Furthermore, by using an antibody

named VRQ14, specific to extractive PrP^C, a crystallography structure of the complex VRQ14:recPrP has been obtained at 2.5 Å resolution [53]. The structure of the complex allowed to state that the tertiary structure of extractive PrP^C and recPrP are identical. The fold-equivalence between extractive PrP^C and recPrP is not very surprising. Indeed, by taking into account the fact that PrP protein has only two cysteines both located in the globular domain and forming the unique PrP disulfide bridge which direct the PrP α-fold makes it highly unlikely that two different α-fold conformations could coexist. Furthermore, structural investigations highlighted that the H2H3 domain of PrP constitutes an independent folding unit [54] forming spontaneously an α-fold. The aggregation pathway of recPrP is also equivalent to PrP^C. Indeed, a plethora of publications now report the use of recPrP in *bona fide* prion conversion methods [55]. For all these reasons we estimate that most of the observations made on recPrP are biologically reliable which does not exclude that other cell cofactors can affect observations.

Consequently, our results were considered consistent. With regards to PrP disease the connection of our results is made by our recent finding that PrP is represented by, at least, three conformers in equilibrium and that these last exchange structural information that modify the conformational equilibrium [18]. Under these circumstances a change of the environment, or the appearance of a mutation was shown to disrupt this equilibrium that could be an entry point towards the prion disease emergence. To conclude, our results undoubtedly reflect the effect of oxidative stress upon prion conformational properties that are connected to prion diseases.

The formation of precipitate at pH 7 and not at pH 3.9 is likely very relevant from a biological point of view. Unfortunately, most of the tools that were intended to be used for this study (SEC, IMS/MS, CD, AFM) are adapted to the study of solubilized protein or protein aggregates. The processes leading to this precipitation under irradiation at pH 7 can only be speculated: although on the initial, monomeric, conformation equilibrium, no significant pH effect was observed [27], irradiation seems to trigger a sudden precipitation process.

Thus, the main findings of this work are i) that oxidation promotes the formation of molecular assemblies, ii) that these molecular assemblies contain both oxidized and intact monomers at low irradiation dose, iii) that the PrP proteins remaining in the monomer form are those who do not incorporate a +16 Da shift, tell-tale of oxidation by O addition. The presence of intact and oxidized monomers constituting the molecular assemblies is in sharp contrast with experiments reporting modifications using hydrogen peroxide in high amounts in the presence or absence of cations. In the latter cases the unique detection of oxidized monomers could be due to the excess of the chemical reagents employed to this end. Two main possibilities seem to be suitable to explain the overserved results; i) intact monomers are recruited by oxidized monomers that promote structural changes of the latter via a structural information transfer or ii) intact monomers having intrinsic capability spontaneously associate with modified monomers. Our experiments did not allow to rule out one of these hypotheses. These results also suggest that chemical modifications triggered by ROS not only chemically modify PrP but also disrupt its conformational equilibrium. Such assumption can be connected to a recent work of our group showing that factors, like protein concentration changes, modulate the conformerôs abundances through the formation of transient multimers those exchanging structural information [18]. Many reports show that oxidized monomers possessed a β-rich structure, as it should be the case for oxidized monomers embedded in molecular assemblies [56]. Consequently, we can assume that intact monomers in the molecular assemblies probably share the same structural properties. However, CD measurements did not indicate a conformational change of PrP towards a more β-sheet rich structure whereas β-sheet rich structures are typically observed when oxidizing PrP (see Table 1). Since CD measurements are bulk measurements, the low relative amount of modified PrP (approximately ~ 2% at a bulk sample concentration of 100 µM and a 100 Gy irradiation dose) could prevent the observation of a significant shift in the CD spectra. Consequently, the detailed nature of the structure of the intact and modified monomers (MAm) remains elusive [1, 57]. The molecular assemblies in the scope of this work may act as interesting candidates for *in vivo* investigations. Finally, AFM results demonstrate that irradiation promotes a gradual appearance of larger objects in agreement with the observation of MA (Figure 5).

From a biological point of view, we can assume that an increase in the amount of molecular assemblies in cells could be related to ROS bursts. Since the amount of molecular assemblies (relative ratio) increase up to 50 Gy and are rather constant at higher doses this means that accumulation of molecular assemblies does not depend on the irradiation dose after 50 Gy (~ 27.5 µM cumulative $OH^{\bullet}$) and consequently on hydroxyl radical production (e.g. 100 Gy = ~ 55 µM cumulative $OH^{\bullet}$). As mentioned previously, hydroxyl radical is the most reactive ROS, with respect to its reaction rate of 10^8 to 10^{10} $mol^{-1}.l.s^{-1}$. Its reactivity is only limited by its diffusion rate in the aqueous medium. Under these

circumstances its lifetime is very short and below the tens of microseconds with accessible distances of only few nanometers, thus only reacting with molecules in its vicinity. Consequently, an increase in the amount of molecular assemblies in cells could be related to accumulation of ROS bursts.

Finally, ion mobility data allowed obtaining a partial view of the structural dynamics of PrP under oxidation. In the absence of additional data, we must state here that this discussion is quite speculative at some points. Thus, although they are quite distant (as they arise from gas phase dissociation of the MA), CCSs were found to be similar for both MAm with or without mass increments indicating occurrence of oxidative processes, suggesting that they share some structural features whether modified or not. In contrast, for higher irradiation doses, CCSs were found smaller than those at 7 Gy. This could suggest that a transition in the MA structure occurs when more oxidized monomer are produced. However, in a quantitative point of view, M conformers were shown to undergo changes in their respective abundances with respect to irradiation dose. This result is explained by the disruption of the conformational equilibrium of the prion via structural information transfer. In other words, molecular assemblies (MA) by interacting with other monomers (M) in the solution quantitatively probably modify the conformational profile of the latter. This result is in full agreement with our recent work demonstrating that conformersô equilibrium depends on structural information exchanges via the formation of transient multimers promoting conformational changes in individual conformers. This discovery sheds a new light on the possible origin of prion diseases, namely that a change in prion structure could be transmitted through the formation of transient multimers either by protein concentration change but also through oxidative stress [18].

5. Conclusions

To conclude, our results using γ-irradiation to generate ROS clearly demonstrated that the use of mild oxidation conditions in the absence of oxygen allows to investigate oxidation-prone alterations, without modifying the protein matrix. Oxidative stress was shown to lead to the production of molecular assemblies that could be related to PrP neurotoxicity. The presence of oxidized and non-oxidized PrP monomers in the evolving molecular assemblyôs species at low irradiation dose shows that the initial steps of protein ñoligomerizationò are more complex than previously thought. This event is proposed to be the early step leading to the formation of oligomers. Last but not the least, this study showed that intact monomers in molecular assemblies are selected either by a conformational selection of the monomers having a structure compatible with oxidized monomers or via structural information transfer from oxidized monomer toward intact monomers. To this extent it will be of great interest to test the biological activity of these heterogeneous PrP assemblies. The results also show that the conformational landscape of PrP plays a role in the formation of these assemblies. In this case molecular assemblies are likely produced according to a structural process that differs from thermal denaturation [56]. These results demonstrate that the presence of molecular assemblies lead to a resampling of the conformational equilibrium of the intact monomers (M) without promoting their fall out in ñpathogenic speciesò. Finally, the attempts to irradiate at pH 7 pave the way for further experiments based on separate techniques, which require either re-solubilization of the precipitate, which will lead to a loss of the conformational properties and of the size of putative oligomeric intermediates in the precipitation pathway, or a direct study of the solid phase precipitate using alternative solid-state techniques (SAXS, NMR, AFM-IR).

Acknowledgements: The authors acknowledge the funding by the Ile-de-France DIM Analytics program for the MOBICS project.

Declaration of interest: None.

Authors contribution: FH conceptualized the scientific hypothesis, ran the experiments, analyzed the data and wrote, reviewed and edited the paper. CS performed samples irradiations, participated to scientific discussion, and review of the paper. GvDR, participated to scientific discussion and to the writing, review and editing of the paper. JB ran AFM experiments and part of the IMS-MS experiments, and was involved in the writing and review of the paper. HR, supplied the recombinant protein and participated to scientific discussion.

References

[1] L. Redecke, M. von Bergen, J. Clos, P.V. Konarev, D.I. Svergun, U.E. Fittschen, J.A. Broekaert, O. Bruns, D. Georgieva, E. Mandelkow, N. Genov, C. Betzel, Structural characterization of beta-sheeted oligomers formed on the pathway of oxidative prion protein aggregation in vitro, J Struct Biol 157(2) (2007) 308-20.

[2] K.N. Prasad, S.C. Bondy, Oxidative and Inflammatory Events in Prion Diseases: Can They Be Therapeutic Targets?, Curr Aging Sci 11(4) (2019) 216-225.

[3] L. Westergard, H.M. Christensen, D.A. Harris, The cellular prion protein (PrP(C)): its physiological function and role in disease, Biochim Biophys Acta 1772(6) (2007) 629-44.

[4] F. Collin, C. Cheignon, C. Hureau, Oxidative stress as a biomarker for Alzheimer's disease, Biomark Med 12(3) (2018) 201-203.

[5] N. Hettiarachchi, M. Dallas, M. Al-Owais, H. Griffiths, N. Hooper, J. Scragg, J. Boyle, C. Peers, Heme oxygenase-1 protects against Alzheimer's amyloid-beta(1-42)-induced toxicity via carbon monoxide production, Cell Death Dis 5 (2014) e1569.
[6] L.D. Coles, P.J. Tuite, G. Oz, U.R. Mishra, R.V. Kartha, K.M. Sullivan, J.C. Cloyd, M. Terpstra, Repeated-Dose Oral N-Acetylcysteine in Parkinson's Disease: Pharmacokinetics and Effect on Brain Glutathione and Oxidative Stress, J Clin Pharmacol 58(2) (2018) 158-167.
[7] N. Shiraishi, Y. Inai, W. Bi, M. Nishikimi, Fragmentation and dimerization of copper-loaded prion protein by copper-catalysed oxidation, Biochem J 387(Pt 1) (2005) 247-55.
[8] N.D. Younan, R.C. Nadal, P. Davies, D.R. Brown, J.H. Viles, Methionine oxidation perturbs the structural core of the prion protein and suggests a generic misfolding pathway, J Biol Chem 287(34) (2012) 28263-75.
[9] B. Feng, Z. Wang, T. Liu, R. Jin, S. Wang, W. Wang, G. Xiao, Z. Zhou, Methionine oxidation accelerates the aggregation and enhances the neurotoxicity of the D178N variant of the human prion protein, Biochim Biophys Acta 1842(12 Pt A) (2014) 2345-56.
[10] M.I. Elmallah, U. Borgmeyer, C. Betzel, L. Redecke, Impact of methionine oxidation as an initial event on the pathway of human prion protein conversion, Prion 7(5) (2013) 404-11.
[11] J.R. Requena, M.N. Dimitrova, G. Legname, S. Teijeira, S.B. Prusiner, R.L. Levine, Oxidation of methionine residues in the prion protein by hydrogen peroxide, Arch Biochem Biophys 432(2) (2004) 188-95.
[12] Z. Wang, B. Feng, G. Xiao, Z. Zhou, Roles of methionine oxidation in E200K prion protein misfolding: Implications for the mechanism of pathogenesis in E200K linked familial Creutzfeldt-Jakob disease, Biochim Biophys Acta 1864(4) (2016) 346-58.
[13] C. Wolschner, A. Giese, H.A. Kretzschmar, R. Huber, L. Moroder, N. Budisa, Design of anti- and pro-aggregation variants to assess the effects of methionine oxidation in human prion protein, Proc Natl Acad Sci U S A 106(19) (2009) 7756-61.
[14] S.R. Abdelraheim, S. Kralovicova, D.R. Brown, Hydrogen peroxide cleavage of the prion protein generates a fragment able to initiate polymerisation of full length prion protein, Int J Biochem Cell Biol 38(8) (2006) 1429-40.
[15] K. Bobrowski, Radiation chemistry of liquid systems, Applications of ionizing radiation in materials processing (Chapter 4) (2014) 81-116.
[16] E. Brun, Y. Blouquit, P. Duchambon, C. Malosse, J. Chamot-Rooke, C. Sicard-Roselli, Oxidative stress induces mainly human centrin 2 polymerisation, Int J Radiat Biol 86(8) (2010) 657-68.
[17] A. Et Taouil, E. Brun, P. Duchambon, Y. Blouquit, M. Gilles, E. Maisonhaute, C. Sicard-Roselli, How protein structure affects redox reactivity: example of Human centrin 2, Phys Chem Chem Phys 16(44) (2014) 24493-8.
[18] G. Van der Rest, H. Rezaei, F. Halgand, Transient multimers modulate conformer abundances of prion protein monomer through conformational selection, Sci Rep 9(1) (2019) 12159.
[19] A.C. Leney, A.J. Heck, Native Mass Spectrometry: What is in the Name?, J Am Soc Mass Spectrom 28(1) (2017) 5-13.
[20] M. Sharon, C.V. Robinson, The role of mass spectrometry in structure elucidation of dynamic protein complexes, Annu Rev Biochem 76 (2007) 167-93.
[21] S.E. Ahnert, J.A. Marsh, H. Hernandez, C.V. Robinson, S.A. Teichmann, Principles of assembly reveal a periodic table of protein complexes, Science 350(6266) (2015) aaa2245.
[22] S. Mehmood, T.M. Allison, C.V. Robinson, Mass spectrometry of protein complexes: from origins to applications, Annu Rev Phys Chem 66 (2015) 453-74.
[23] A. Politis, C. Schmidt, E. Tjioe, A.M. Sandercock, K. Lasker, Y. Gordiyenko, D. Russel, A. Sali, C.V. Robinson, Topological models of heteromeric protein assemblies from mass spectrometry: application to the yeast eIF3:eIF5 complex, Chem Biol 22(1) (2015) 117-28.
[24] S.H. Chen, D.H. Russell, How Closely Related Are Conformations of Protein Ions Sampled by IM-MS to Native Solution Structures?, J Am Soc Mass Spectrom 26(9) (2015) 1433-43.
[25] J. Seo, W. Hoffmann, S. Warnke, M.T. Bowers, K. Pagel, G. von Helden, Retention of Native Protein Structures in the Absence of Solvent: A Coupled Ion Mobility and Spectroscopic Study, Angew Chem Int Ed Engl 55(45) (2016) 14173-14176.
[26] F. Lanucara, S.W. Holman, C.J. Gray, C.E. Eyers, The power of ion mobility-mass spectrometry for structural characterization and the study of conformational dynamics, Nat Chem 6(4) (2014) 281-94.
[27] G. Van der Rest, H. Rezaei, F. Halgand, Monitoring Conformational Landscape of Ovine Prion Protein Monomer Using Ion Mobility Coupled to Mass Spectrometry, J Am Soc Mass Spectrom 28(2) (2017) 303-314.
[28] R. Cumeras, E. Figueras, C.E. Davis, J.I. Baumbach, I. Gracia, Review on ion mobility spectrometry. Part 2: hyphenated methods and effects of experimental parameters, Analyst 140(5) (2015) 1391-410.
[29] R. Cumeras, E. Figueras, C.E. Davis, J.I. Baumbach, I. Gracia, Review on ion mobility spectrometry. Part 1: current instrumentation, Analyst 140(5) (2015) 1376-90.
[30] K. Giles, S.D. Pringle, K.R. Worthington, D. Little, J.L. Wildgoose, R.H. Bateman, Applications of a travelling wave-based radio-frequency-only stacked ring ion guide, Rapid Commun Mass Spectrom 18(20) (2004) 2401-14.

[31] A.B. Kanu, P. Dwivedi, M. Tam, L. Matz, H.H. Hill, Jr., Ion mobility-mass spectrometry, J Mass Spectrom 43(1) (2008) 1-22.
[32] D.P. Smith, T.W. Knapman, I. Campuzano, R.W. Malham, J.T. Berryman, S.E. Radford, A.E. Ashcroft, Deciphering drift time measurements from travelling wave ion mobility spectrometry-mass spectrometry studies, Eur J Mass Spectrom (Chichester, Eng) 15(2) (2009) 113-30.
[33] Y. Zhao, A. Singh, L. Li, R.J. Linhardt, Y. Xu, J. Liu, R.J. Woods, I.J. Amster, Investigating changes in the gas-phase conformation of Antithrombin III upon binding of Arixtra using traveling wave ion mobility spectrometry (TWIMS), Analyst 140(20) (2015) 6980-9.
[34] W.P. Griffith, I.A. Kaltashov, Highly asymmetric interactions between globin chains during hemoglobin assembly revealed by electrospray ionization mass spectrometry, Biochemistry 42(33) (2003) 10024-33.
[35] L. Han, B.T. Ruotolo, Ion Mobility-Mass Spectrometry Differentiates Protein Quaternary Structures Formed in Solution and in Electrospray Droplets, Anal Chem 87(13) (2015) 6808-13.
[36] A. D'Urzo, A. Konijnenberg, G. Rossetti, J. Habchi, J. Li, P. Carloni, F. Sobott, S. Longhi, R. Grandori, Molecular basis for structural heterogeneity of an intrinsically disordered protein bound to a partner by combined ESI-IM-MS and modeling, J Am Soc Mass Spectrom 26(3) (2015) 472-81.
[37] G.R. Hilton, K. Thalassinos, M. Grabenauer, N. Sanghera, S.E. Slade, T. Wyttenbach, P.J. Robinson, T.J. Pinheiro, M.T. Bowers, J.H. Scrivens, Structural analysis of prion proteins by means of drift cell and traveling wave ion mobility mass spectrometry, J Am Soc Mass Spectrom 21(5) (2010) 845-54.
[38] W. Kaaki, M. Woudstra, B. Gontero, F. Halgand, Exploration of CP12 conformational changes and of quaternary structural properties using electrospray ionization traveling wave ion mobility mass spectrometry, Rapid Commun Mass Spectrom 27(1) (2013) 179-86.
[39] V.N. Uversky, A.K. Dunker, Multiparametric analysis of intrinsically disordered proteins: looking at intrinsic disorder through compound eyes, Anal Chem 84(5) (2012) 2096-104.
[40] H. Rezaei, D. Marc, Y. Choiset, M. Takahashi, G. Hui Bon Hoa, T. Haertle, J. Grosclaude, P. Debey, High yield purification and physico-chemical properties of full-length recombinant allelic variants of sheep prion protein linked to scrapie susceptibility, Eur J Biochem 267(10) (2000) 2833-9.
[41] M.F. Bush, I.D. Campuzano, C.V. Robinson, Ion mobility mass spectrometry of peptide ions: effects of drift gas and calibration strategies, Anal Chem 84(16) (2012) 7124-30.
[42] R. Salbo, M.F. Bush, H. Naver, I. Campuzano, C.V. Robinson, I. Pettersson, T.J. Jorgensen, K.F. Haselmann, Traveling-wave ion mobility mass spectrometry of protein complexes: accurate calibrated collision cross-sections of human insulin oligomers, Rapid Commun Mass Spectrom 26(10) (2012) 1181-93.
[43] B.T. Ruotolo, J.L. Benesch, A.M. Sandercock, S.J. Hyung, C.V. Robinson, Ion mobility-mass spectrometry analysis of large protein complexes, Nat Protoc 3(7) (2008) 1139-52.
[44] A.A. Shvartsburg, R.D. Smith, Fundamentals of traveling wave ion mobility spectrometry, Anal Chem 80(24) (2008) 9689-99.
[45] R. Beveridge, L.G. Migas, K.A. Payne, N.S. Scrutton, D. Leys, P.E. Barran, Mass spectrometry locates local and allosteric conformational changes that occur on cofactor binding, Nat Commun 7 (2016) 12163.
[46] M. Hardy, J. Zielonka, H. Karoui, A. Sikora, R. Michalski, R. Podsiadly, M. Lopez, J. Vasquez-Vivar, B. Kalyanaraman, O. Ouari, Detection and Characterization of Reactive Oxygen and Nitrogen Species in Biological Systems by Monitoring Species-Specific Products, Antioxid Redox Signal 28(15) (2018) 1416-1432.
[47] C. Houée-Levin, Bobrowski K., The use of the methods of radiolysis to explore the mechanisms of free radical modifications in proteins., J Proteomics. (2013).
[48] B. Kalyanaraman, G. Cheng, M. Hardy, O. Ouari, B. Bennett, J. Zielonka, Teaching the basics of reactive oxygen species and their relevance to cancer biology: Mitochondrial reactive oxygen species detection, redox signaling, and targeted therapies, Redox Biol 15 (2018) 347-362.
[49] K.J. Knaus, M. Morillas, W. Swietnicki, M. Malone, W.K. Surewicz, V.C. Yee, Crystal structure of the human prion protein reveals a mechanism for oligomerization, Nat Struct Biol 8(9) (2001) 770-4.
[50] N. Felitsyn, E.N. Kitova, J.S. Klassen, Thermal decomposition of a gaseous multiprotein complex studied by blackbody infrared radiative dissociation. Investigating the origin of the asymmetric dissociation behavior, Anal Chem 73(19) (2001) 4647-61.
[51] D.R. Brown, Neurodegeneration and oxidative stress: prion disease results from loss of antioxidant defence, Folia Neuropathol 43(4) (2005) 229-43.
[52] S. Hornemann, C. Schorn, K. Wuthrich, NMR structure of the bovine prion protein isolated from healthy calf brains, EMBO Rep 5(12) (2004) 1159-64.
[53] F. Eghiaian, J. Grosclaude, S. Lesceu, P. Debey, B. Doublet, E. Treguer, H. Rezaei, M. Knossow, Insight into the PrPC-->PrPSc conversion from the structures of antibody-bound ovine prion scrapie-susceptibility variants, Proc Natl Acad Sci U S A 101(28) (2004) 10254-9.
[54] M. Adrover, K. Pauwels, S. Prigent, C. de Chiara, Z. Xu, C. Chapuis, A. Pastore, H. Rezaei, Prion fibrillization is mediated by a native structural element that comprises helices H2 and H3, J Biol Chem 285(27) (2010) 21004-12.

[55] H. Erana, J.M. Charco, M.A. Di Bari, C.M. Diaz-Dominguez, R. Lopez-Moreno, E. Vidal, E. Gonzalez-Miranda, M.A. Perez-Castro, S. Garcia-Martinez, S. Bravo, N. Fernandez-Borges, M. Geijo, C. D'Agostino, J. Garrido, J. Bian, A. Konig, B. Uluca-Yazgi, R. Sabate, V. Khaychuk, I. Vanni, G.C. Telling, H. Heise, R. Nonno, J.R. Requena, J. Castilla, Development of a new largely scalable in vitro prion propagation method for the production of infectious recombinant prions for high resolution structural studies, PLoS Pathog 15(10) (2019) e1008117.
[56] H. Rezaei, F. Eghiaian, J. Perez, B. Doublet, Y. Choiset, T. Haertle, J. Grosclaude, Sequential generation of two structurally distinct ovine prion protein soluble oligomers displaying different biochemical reactivities, J Mol Biol 347(3) (2005) 665-79.
[57] F. Eghiaian, T. Daubenfeld, Y. Quenet, M. van Audenhaege, A.P. Bouin, G. van der Rest, J. Grosclaude, H. Rezaei, Diversity in prion protein oligomerization pathways results from domain expansion as revealed by hydrogen/deuterium exchange and disulfide linkage, Proc Natl Acad Sci U S A 104(18) (2007) 7414-9.

Figures:

Figure 1: A) UV trace (UV DAD 210 ï 300 nm) of PrP SEC fractionation before and after irradiation (100 Gy) at pH 3.9, displaying the presence of another peak corresponding to molecular assemblies (MA). B) Evolution of the relative intensities (UV DAD 210 ï 300 nm) for monomers, dimers and molecular assemblies as a function of the irradiation dose. C) Same graph as in B) but without the monomer bars. (color figure)

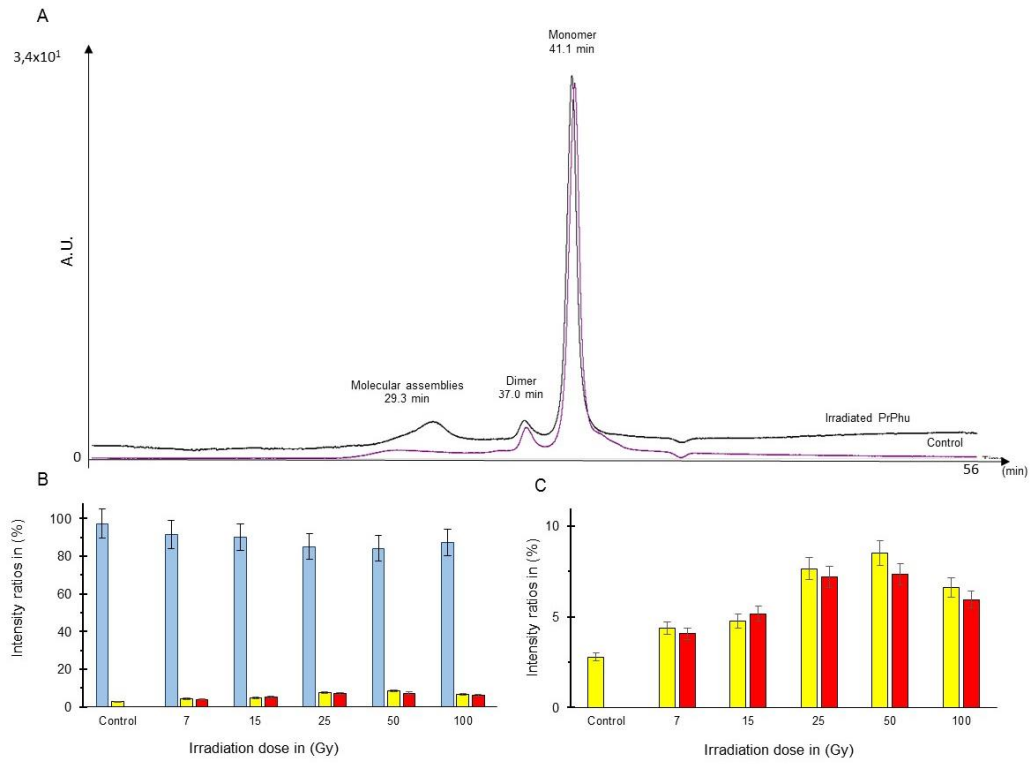

Figure 2: A) SDS PAGE of PrP 30 µM in KH_2PO_4 10 mM pH 3.9. 10 µl of denatured PrP at 15 µM were loaded on the gel. Two lanes on the right correspond to the same experiment in the absence of DTT. B) SEC-MS spectra of the dissociated monomers from of the molecular assembly peak (50 Gy, red trace) and monomer from monomer peak (blue trace, dose 50 Gy) and the (red curve, dose 50 Gy) under native conditions. C) Mass spectra overlay of the control (blue trace) and irradiated monomer (red trace) under native conditions. See insert for a detailed view of the +6 charge state. D) Mass spectra overlay of the irradiated monomer (blue trace) and the dissociated monomers (red trace) from of the molecular assemblies under denaturing conditions. See insert for a detailed view of the +14 charge state.

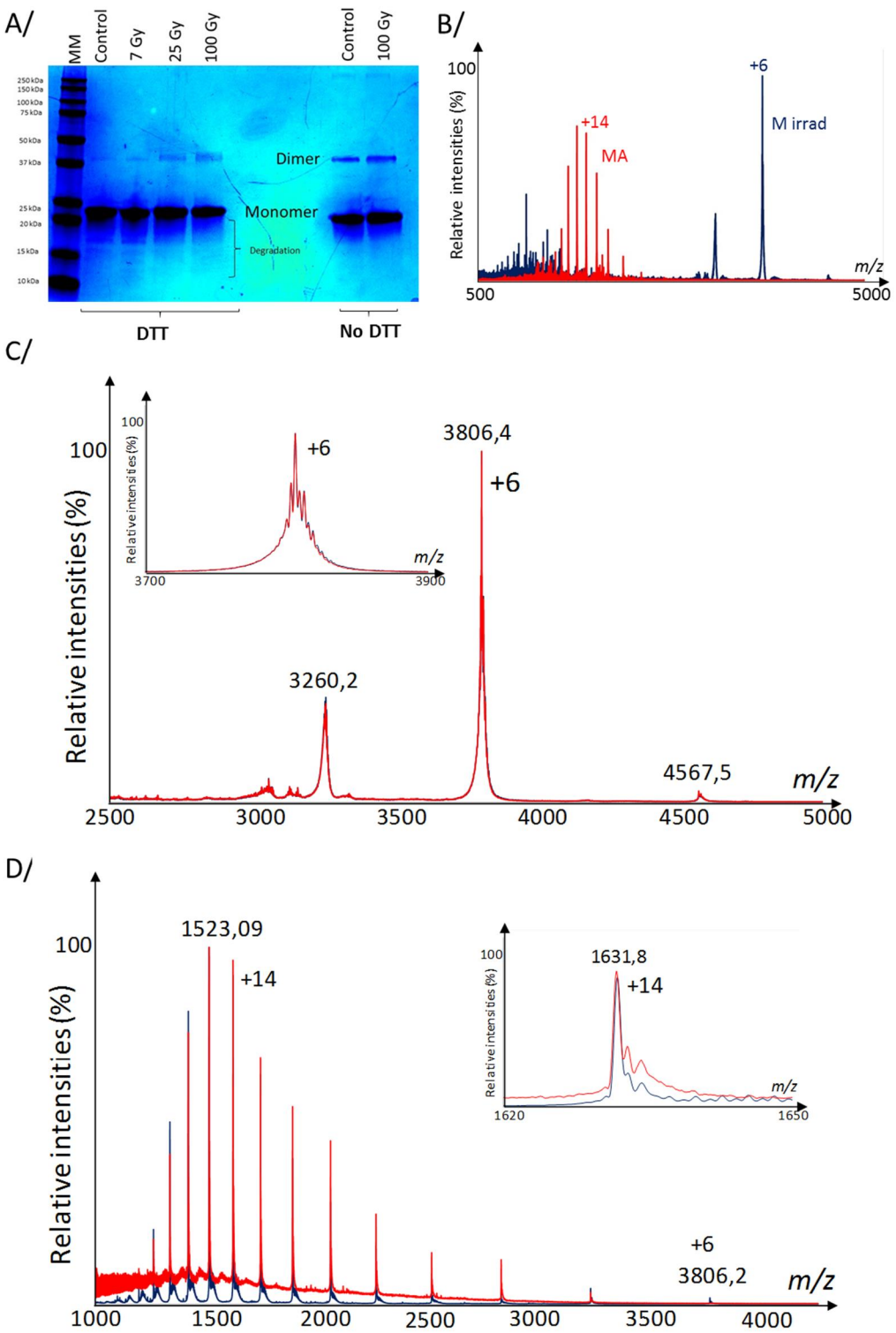

Figure 3: Mass spectrum of molecular assemblies of PrP reconstructed from molecular assembly peak (Top panel). Monomers present in the spectra are the product of gas-phase dissociation. Black spheres indicate charge states of PrP. In the zoom (red box) a charge state distribution for an octamer is indicated (~182 KDa).

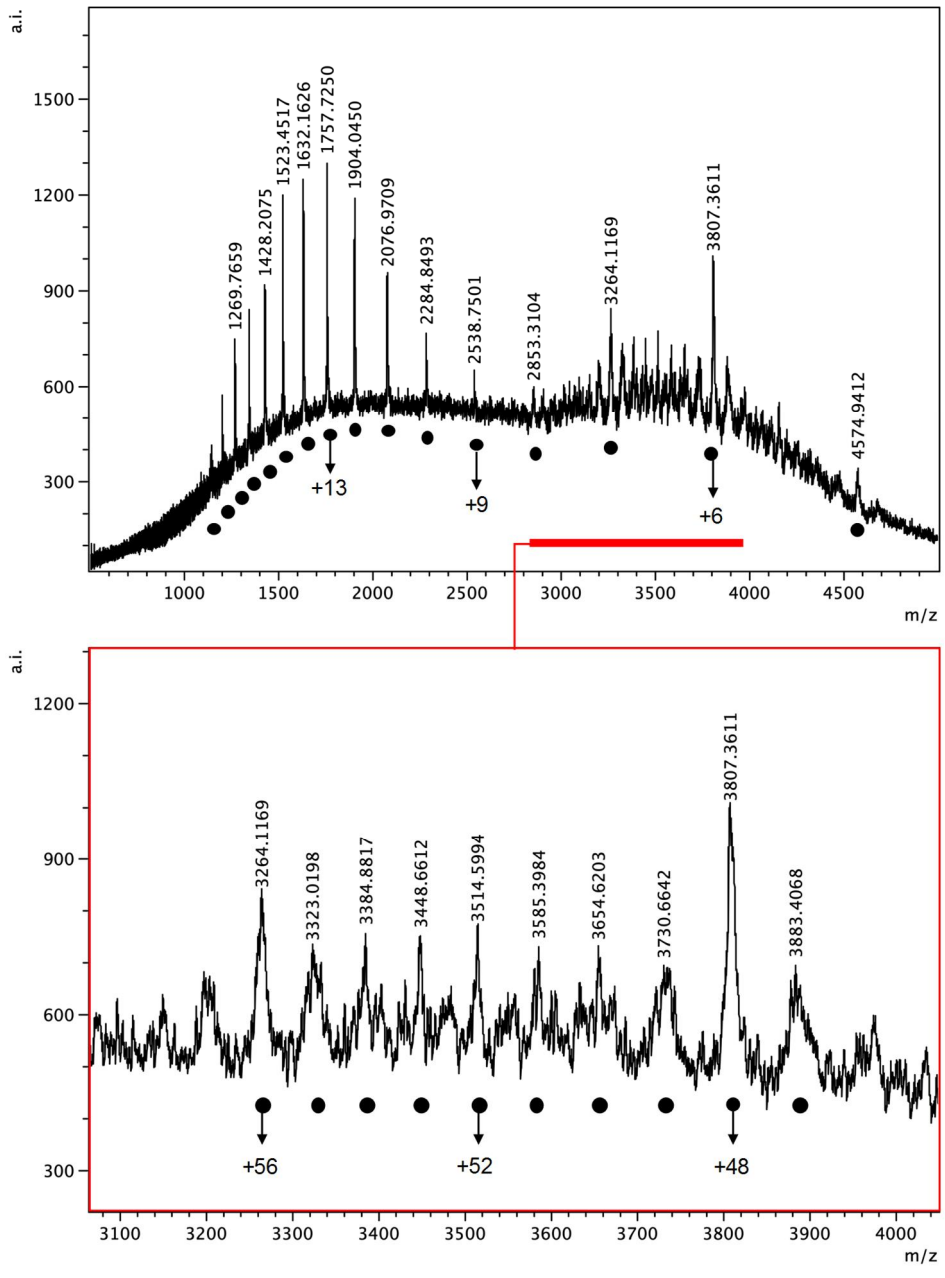

Figure 4: A/ Plot of the CCS as a function of charge states (CCS = f (z)) of control (MCtrl) and irradiated PrP (Mirr and MAm). B/ Plot of the relative abundances of monomer (MCtrl and Mirr) conformers as a function of the irradiation dose. *Legends*: MAm = monomer of molecular assemblies displaying or not mass increment (ex: MAm 100 Gy Δ 41 Da); Irradiation dose is given for each sample; M monomer (Ctrl control without irradiation; in Gy the irradiation dose).

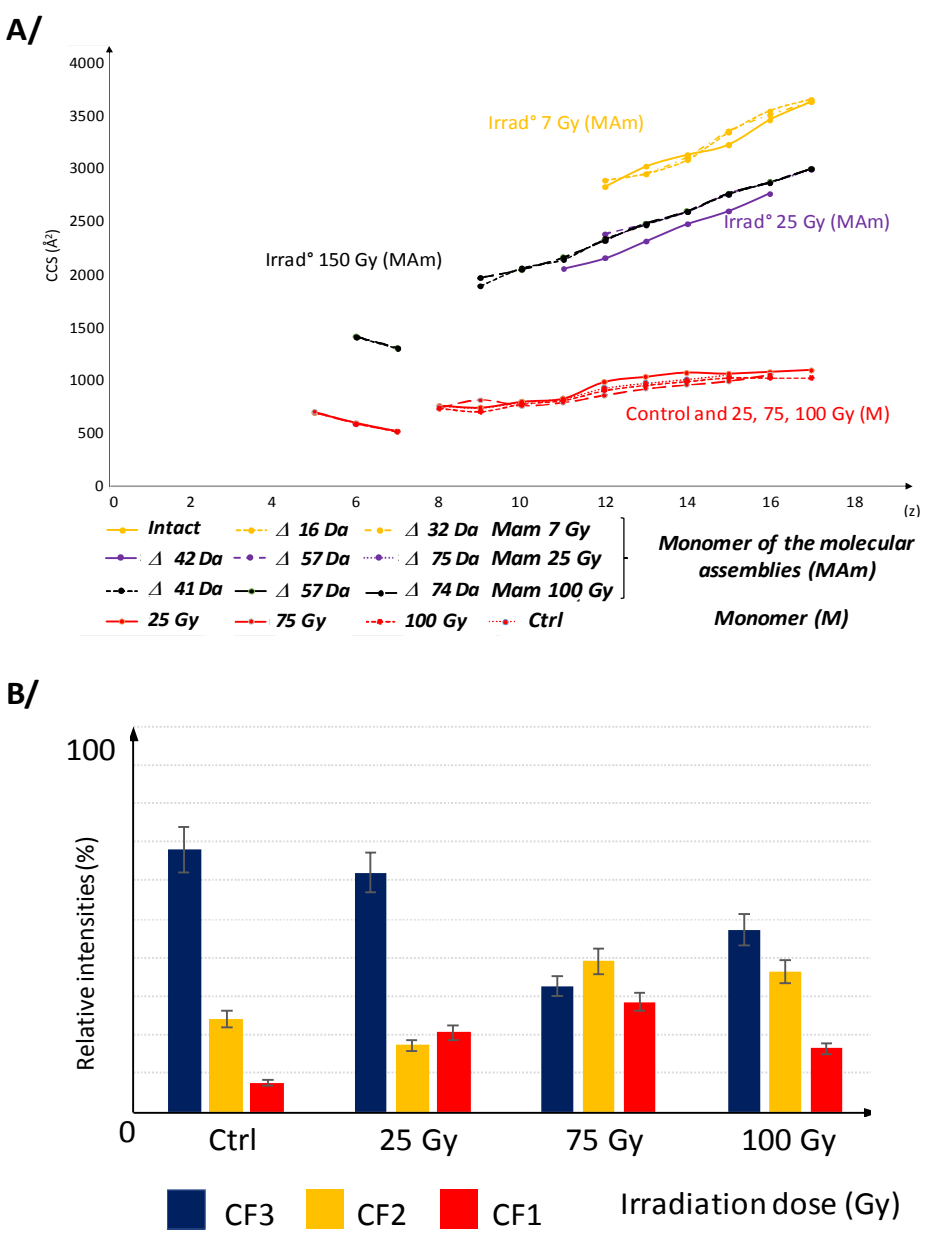

Figure 5: A/ AFM micrographs of bulk PrP solution irradiated with doses 0, 25, 100 and 200 Gy and imaged in solution. Samples were diluted to 250 nM in 5 mM KH_2PO_4 pH 3.9. B/ Bar graphs indicate the heights of the objects with respect to control and irradiation at 25, 100, 200 Gy. Inserts allows to focus on objects of bigger size.

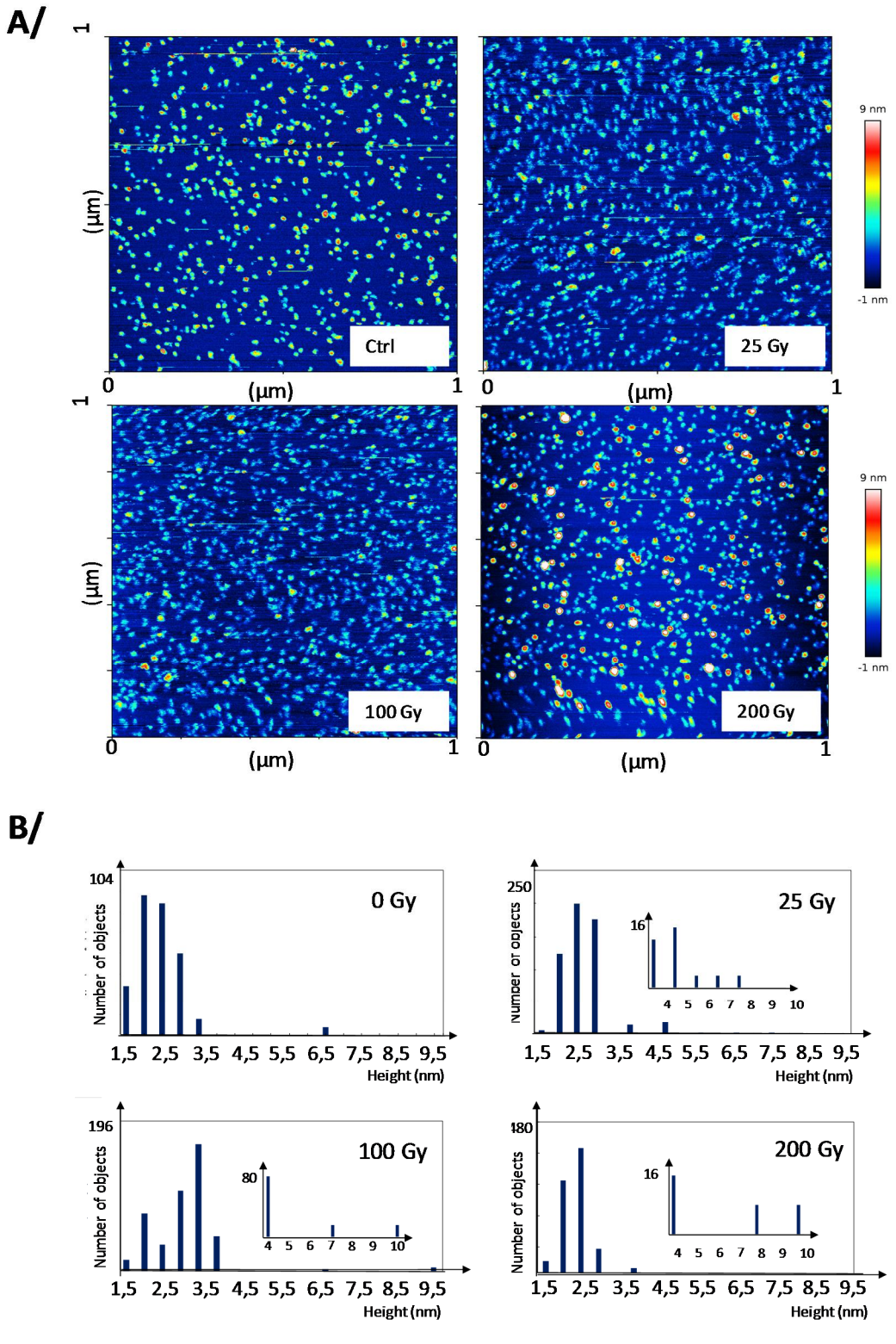

Table 1: Overview about publications on the oxidation of PrP.

Protein	Protein conc.	Buffer	Oxidizing agent/Conc.	Change □->ϐ	Aggregates	Reference
Human PrP, 121-213	44 µM	10 mM NaAc, pH 5	Cu pellets, 16 mg/60 µl, 37°C, 1 hr	✓	✓	Elmallah *et al. [10]*
Human PrP, 1-253 D178N	35 µM	25 mM Na_3PO_4, pH 6	50 mM H_2O_2, 37°C, 1-20 hrs	✓	✓	Feng *et al. [9]*
Hamster PrP, 29-231	3.5 µM	10 mM Na3PO4, pH 7.2	3-10 mM H_2O_2, 37°C, 15 min	✓	✓	Requena *et al.[11]*
Human PrP, 23-231	400 µM	10 mM MES pH 6	0.5-25 eq. $NaIO_4$, 0°C, >12 hrs	✓	✓	Wolschner *et al. [13]*
Mouse PrP 23-231	4-130 mM	19 mM NaAc pH 5.6	10 mM H_2O_2, 0.1 mol eq. Cu^{2+}, 16 hrs	✓	✓	Younan *et al. [8]*
Human PrP, 1-253	50 µM	25 mM Na_3PO_4, pH 6	50 mM H_2O_2, 37°C, 2-12 hrs	✓	✓	Wang *et al. [12]*